Journal of Innovative Materials in Extreme Conditions
2023
Volume 4
Issue 1

DATA-MINING *AB INITIO* STUDY OF GYPSUM AND $CaCO_3$ MODIFICATIONS AT STANDARD AND EXTREME CONDITIONS

Tamara Škundrić[1,2,3], Branko Matović [1,2], Aleksandra Zarubica [3], Dorota Chudoba[4], Dejan Zagorac[1,2]

[1]*Institute of Nuclear Sciences "Vinča", University of Belgrade, Belgrade, Serbia*
[2]*Centre of Excellence "Cextreme Lab", Centre for synthesis, processing, and characterization of materials for application in extreme conditions, Belgrade, Serbia*
[3]*Department of Chemistry, Faculty of Science and Mathematics, University of Niš, Niš, Serbia*
[4]*Joint Institute for Nuclear Research (JINR), Frank Laboratory of Neutron Physics, Dubna, Russia*

Corresponding author: tamara.skundric@vin.bg.ac.rs*

Abstract: *Calcium carbonate and gypsum are very common and widespread minerals widely used in many fields. However, in order to investigate their behavior under extreme conditions of pressure and temperature, a data-mining ab initio approach has been performed. To analyze structural stability and explore different $CaCO_3$ and gypsum phases in these extreme conditions, the most interesting modifications have been submitted to the DFT calculations. Local optimizations have been performed using the CRYSTAL17 solid-state-quantum-chemical program. Total energies of different gypsum phases are presented and it seems that among the calcite phases, the Calcite I ($CaCO_3$ I) phase has the lowest calculated total energy using the three different functionals in agreement with experimental data. Each of the modified phases of these minerals has been discussed and presented in this study. Due to the very wide industrial and technological application of these natural minerals, further investigation could be of great importance, especially their performances in extreme environments.*

Keywords**:** *calcium carbonate, gypsum, DFT, crystal structure prediction, data-mining, extreme pressures, high temperatures*

1. Introduction

There are several studies investigating phase transitions in gypsum and calcium carbonate in extreme conditions, using different pressure and temperature ranges within the research. Raman spectroscopy is the most used technique for phase transformations research, often combined with x-ray diffraction [1], or electrical conductivity experiments [2], but to investigate a phase transformation of gypsum into bassanite and anhydrite, one new original apparatus has also been developed, that combines an acoustic levitator and a pressure-compatible process chamber [3].

Results from the experiments indicate that gypsum dissolves in water at ambient temperature and pressure above 496 MPa, but the solubility increases significantly with increasing pressure and finally entirely dissolves at a pressure of around 866 MPa [4]. At the pressure of 2 GPa under cold compression, a phase transition from anhydrite to a monazite type has been observed [1]. However, between 2 and 5 GPa, anhydrite undergoes a gradual phase change from orthorhombic to monoclinic monazite structured phase, with a 6-8% volume change, strongly dependent on pressure [5]. At the higher pressures of 33.2 GPa and after laser heating, another phase transition has been observed and a change in color of the sample is noted, from transparent to black, with an indication that this newly discovered phase can persist to 53.5 GPa and 1800 K [1]. Accordingly, with the pressure of 5,8 GPa and atmospheric temperature, a structural phase transition in gypsum has been confirmed [2]. Thereby, at a relatively low pressure of around 0.3 GPa, starting gypsum transforms to anhydrite in only one step dehydration reaction [2].

However, at the pressure of 2,5 GPa, a two-step dehydration reaction has been confirmed as the gypsum firstly transforms into bassanite, $CaSO_4$ hemihydrate, at around 428 K [6] or 523 K[2], and then completely dehydrates to anhydrite at 673K [2]. According to another study, firstly γ-

anhydrite is formed at 488 K, and then at 593 K γ-anhydrite irreversibly transforms to the β-anhydrite form [6]. At room temperature and a pressure of 2 GPa, a further polymorphic transition of β-anhydrite to monazite has been observed and this transformation is described as completely reversible due to the Raman spectra of recovered samples [6]. Besides, with temperature increase, the anhydrite phase ($CaSO_4$) precipitates at 250-320°C and in the pressure range of 1.0 – 1.5 GPa. Hence, both conditions, a stable range of pressure and temperature along with the supersaturation of Ca and SO_4 ion concentrations in an aqueous solution are crucial for the anhydrite formation [4]. This transition that involves two processes, dissolution, and precipitation is defined as irreversible [4], while anhydrite is also described as a possible oxygen carrier particle (OCP) material [7].

Thus, in extreme conditions of high temperature and pressure, besides the monazite-type, denoted as a metastable phase to pressures up to almost 30 GPa [5], barite-type phases have also been found, and these phases are described as mechanically stable polymorphs of the ambient phases – anhydrite [8]. There is also a suggestion that anhydrite and monazite-structured phases are the only phases that can be observed under shock loading of $CaSO_4$ to pressures above 100 GPa [5]. However, even at room temperature, a phase transition from anhydrite to monazite can be induced by a pressure of around 3 GPa [8]. However, the transition from monazite to barite requires higher temperatures (>1500 K and ~20 GPa), though this phase cannot always be quenched from high temperatures, and can be distorted to some other structures as well [8]. According to the Raman and Infrared spectra of gypsum at high pressures, up to 21 GPa and 300 K, gypsum retains molecular-like sulphate groups and water molecules to pressures up to 20 GPa and 300 K [9]. Its water and sulphate vibrations remain discrete, indicating that highly rigid molecular units are maintained throughout this pressure range [9]. Due to the progressive removal of water molecules from the gypsum, the peaks reduce in amplitude and the removal of water molecules affects the crystallographic environment, hence the distortion of the $SO4^{2-}$ tetrahedra [3]. There is also a suggestion that the compression of the monazite structured phase is remarkably anisotropic, as the pressure-induced compaction is mostly accommodated by a and b axes [5].

Calcium carbonate is a very widespread mineral found in the Earth's crust. At atmospheric pressure, it crystalizes in the calcite phase, but with an increase in pressure, this ambient phase of $CaCO_3$ undergoes several phase transitions [10]. Starting from the ambient temperature, at the pressure of 1.7 GPa calcite I transform into calcite II, which further changes to calcite III at the pressure of approximately 2 GPa and this structure can be retained up to at least 10 GPa [11]. Also, using the single-crystal synchrotron X-ray diffraction, high-pressure polymorphs have been detected, $CaCO_3$-III and $CaCO_3$-VI phases [10]. $CaCO_3$ that is noted in the pressure range of 2,5 to 15 GPa is triclinic and presents two closely related structural modifications ($CaCO_3$-III and $CaCO_3$-IIIb) with an indication that different experimental paths can stabilize one or the other polymorph [10].

There is also a report of $CaCO_3$ polymorph found in extreme conditions of pressure and temperature, referred to as a calcite-Vb phase [12]. It occurs at pressures >3,5 GPa and temperatures more than 1200°C, as an intermediate between aragonite and calcite V, and this new $CaCO_3$ phase has the $KClO_3$-type structure and appears in the monoclinic $P2_1/m$ space group [12]. At pressures above 15 GPa up to 40 GPa, a triclinic $CaCO_3$-VI polymorph has been noted with 10 atoms in the unit cell [10]. However, after the pressure release, three phases $CaCO_3$-III, $CaCO_3$-IIIb, and $CaCO_3$-VI transform back to the calcite, with the sample recovered as a single crystal [10]. Additionally, first principle calculations have been performed to calculate the elastic properties for the three high-pressure phases of $CaCO_3$, aragonite, post-aragonite, and *P21/c-h* $CaCO_3$ structure with a conclusion that these high-pressure polymorphs have low isotropic wave velocity and high wave velocity anisotropies [13].

Investigation of the stability of $CaCO_3$ at high pressures and temperatures has also revealed that the $CaCO_3$ in the aragonite structure transforms into $CaCO_3$-VII (*P21/c*) at 27 GPa and 1500 K and it appears that this phase is stable between 23 and 38 GPa at 2300 K while at 42 GPa and 1400 K, it transforms into post-aragonite [14]. Further, by combining the density functional theory with the exchange-correlation functional augmented by the dispersive vdW interaction with quasi-harmonic approximations, the thermodynamic properties of $CaCO_3$ phases have been calculated and the *P*21/*c*-*l* phase has a very narrow region of stability, according to the results [15]. Besides, these simulations also suggested that this *P*21/*c*-*l* phase is structurally identical to the $CaCO_3$-VII phase [15], which is

also in agreement with some previous results [14, 16]. In 2020, a newly discovered phase named disarag, have been found, and described as a dynamically disordered aragonite with freely rotating CO_3 groups which is similar to that in the $CaCO_3$-V phase with a calcite-like structure [17]. This new phase, disarag is referred to as a stable phase in the pressure range of 3 to 10 GPa and from 1600 to 2000K [17]. Also, the increase of temperature at 3,4, and 6 GPa, led to a series of transitions starting from calcite that transformed to aragonite, which further changed to disordered calcite and finally to liquid, and upon rapid cooling of the liquid, aragonite was retained [11]. Besides the earlier known calcite-type disordered structures such as $CaCO_3$-IV, $CaCO_3$-V, rhombohedral $SrCO_3$, rhombohedral $BaCO_3$, and cubic $BaCO_3$, the existence of the disordered aragonite has been also proved, though at the high pressures [17].

Moreover, a reversible temperature-induced aragonite-amorphization transition in $CaCO_3$ has been found at 3.9 to 7.5 GPa and temperatures above 1000K [18]. This amorphous $CaCO_3$ shares a similar structure as liquid $CaCO_3$, but also a mechanism of lattice collapse for the temperature-induced amorphous phase has been suggested [18]. Moreover, using a combination of advanced *ab initio* simulation techniques and high-pressure experiment, a crystal structure of $CaCO_3$ post-aragonite that has been enigmatic for a long time, has been finally determined and this is the phase that is experimentally known to be stable above 40 GPa. [19]. Also, some novel energetically competitive structures have been identified with one of them being even more stable than aragonite above 42 GPa, which appears in the orthorhombic space group *Pmmn* and belongs to a new structure type, which is also adopted by the high-pressure post-aragonite phases of $SrCO_3$ and $BaCO_3$ [19]. When heated to high temperatures (>1500K) and at pressures >130 GPa, calcium carbonate transforms into an orthopyroxene-type structure that is also in agreement with theoretical predictions from *ab initio* calculations [20]. Particularly, at the pressure of 137 GPa, a pyroxene-type structure that appears in the orthorhombic space group *C2221*, becomes more stable than aragonite [19]. Besides the post-aragonite phase with a threefold coordination of carbon cations that manifest strongly anisotropic compressibility of each axis of the unit cell parameter, there is no obvious anisotropy in the pyroxene-type phase [20].

2. Materials and methods

In order to gain insight into the structural stability of the $CaCO_3$ and gypsum phases in extreme conditions of pressure and temperature, a data mining *ab initio* approach has been performed. We performed data-mining-based explorations of the ICSD database [21, 22] via resemblance to known crystallographic structures. A well-known KDD (knowledge discovery in databases) process, which involves selection, preprocessing, transformation, and interpretation/evaluation (or postprocessing) has been used, which also proved to be successful in some previous studies [23-25]. Also, it is of great importance to the effect of extreme conditions on structural properties, as well as the structure-property relationship that has been studied previously [26-30]. All potential structure candidates that have been obtained from data mining search are subsequently submitted to local optimization at an *ab initio* level and a combination of data mining and *ab initio* methods can be found elsewhere [31, 32].

Further, these structure candidates have been submitted to the density functional theory (DFT) calculations and local optimizations (including the cell parameters and atom positions) were performed using the CRYSTAL17 code [33-35], which is based on the linear combination of atomic orbitals. Structure optimizations were performed on the DFT level, employing three different functionals: the Generalized Gradient Approximation (GGA) with the Perdew–Burke–Ernzerhof (PBE) functional [36], the Local Density Approximation (LDA) with the Perdew–Zunger (PZ) correlation functional [37], and the hybrid B3LYP functional (Becke's three-parameter functional in combination with the correlation functional of Lee, Yang, and Parr) [38], for comparison. An all-electron basis set based on Gaussian-type orbitals was employed; in particular, in the case of calcium carbonate modifications, Ca_86-511d3G_catti_1991 for calcium [39], C_6-21G*_catti_1993 for carbon [27, 40] and O_8-411_towler_1994 for oxygen [41, 42] and H_5-11G*_dovesi_1984 for hydrogen [43, 44], respectively. In each structural optimization, Fock/KS matrix mixing was set to 30%, and the tolerances for the convergence on energy were set to 10^{-7}. K-point meshes of 8 _ 8 _ 8

Monkhorst-Pack scheme have been used. A computational strategy implemented in the CRYSTAL17 solid-state, quantum-chemical program has been performed for the accurate *ab initio* simulation of elastic and mechanical properties of crystalline materials [45]. The symmetries of the analyzed structures were determined using the SFND [46] and RGS [47] algorithms implemented in the program KPLOT [48]. The structures were visualized using the Vesta3 program [49].

3. Results and Discussion

Aiming to investigate the structural stability of different gypsum phases in extreme conditions of pressure and temperature, the most interesting formations have been modified. Local optimizations of CaO, CaOH, anhydrite, hemihydrate, and gypsum have been performed using the two different functionals, the GGA-PBE and the LDA-PZ, due to comparison. Calculated total energies and full structural data are given in Tables 1 and 2, respectively.

Table 1. The total energies of the most interesting formations calculated with the GGA-PBE and the LDA-PZ functional. Note that the energies per formula unit are given in hartrees (*Eh*).

Compound/ Modification	Total Energy (*Eh*)	
	GGA-PBE	LDA
CaO	-752.709	-750.663
CaOH	-829.109	-826.592
$CaSO_4$-anhydrite	-1376.289	-1371.709
$CaSO_4$-hemihydrite	-1414.476	-1409.666
$CaSO_4x2H_2O$	-1529.057	-1523.551

The first modification was computed in the CaO chemical system that appears in the rock salt (NaCl) type of structure. The CaO modification shows space group *Fm-3m* (no. 225) with unit cell parameters of a=4.828 Å, calculated with the GGA-PBE functional. Within this cubic structure, calcium ions are in 6-fold coordination by oxygen atoms, thus forming edge-connected octahedra. The distance between atoms is 6 × 2.4144 Å-O, and the structure is presented in Figure 1a. This is in agreement with previous observations [50], and such a structure is capable of withstanding high pressure and temperature conditions.

The next modified structure is CaOH which appears in space group *P-3m1* (no. 164) [51]. This structure is visualized in Figure 1b, with unit cell parameters a=3.613 and c=4.974 Å, calculated with the GGA-PBE functional. Within this trigonal structure, calcium ions are 6-fold coordinated by oxygen and form two layers of edge-connected octahedra with an interatomic distance of 6 × 2.3825 Å-O. The hydrogen atom is connected to only one oxygen atom with a distance between atoms of 0.9857 Å-O.

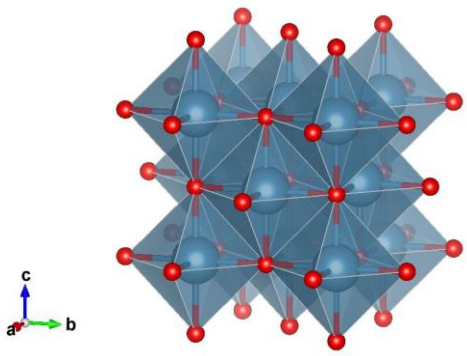

(**a**)

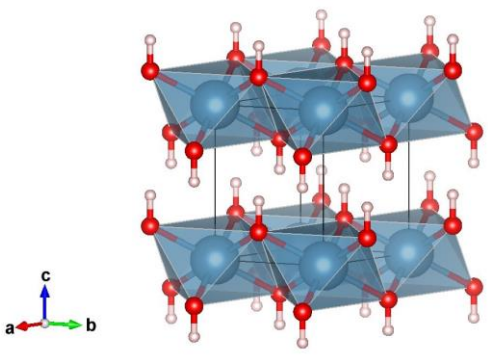

(**b**)

Figure 1. Visualization of the a) CaO that appears in *Fm-3m* (no. 225) and b) CaOH in *P-3m1* (no. 164), calculated with the GGA-PBE functional. Blue, red and pink spheres denote calcium, oxygen, and hydrogen atoms, respectively.

Following modification is a hexagonal calcium sulphate anhydrite that appears in space group *P*6222 (no. 180) and is visualized in Figure 2a [52]. Anhydrite is an anhydrous compound (it does not contain water in its crystal structure), and such is a unique material with outstanding properties beneficial to many industrial applications. This hexagonal structure has unit cell parameters of *a*=7.093 Å and c=6.450 Å, calculated with the GGA-PBE functional, while full structural data are given in Table 2. Sulphur ions are in 4-fold coordination with oxygen and form tetrahedra with an interatomic distance of 4 × 1.5323 Å-O.

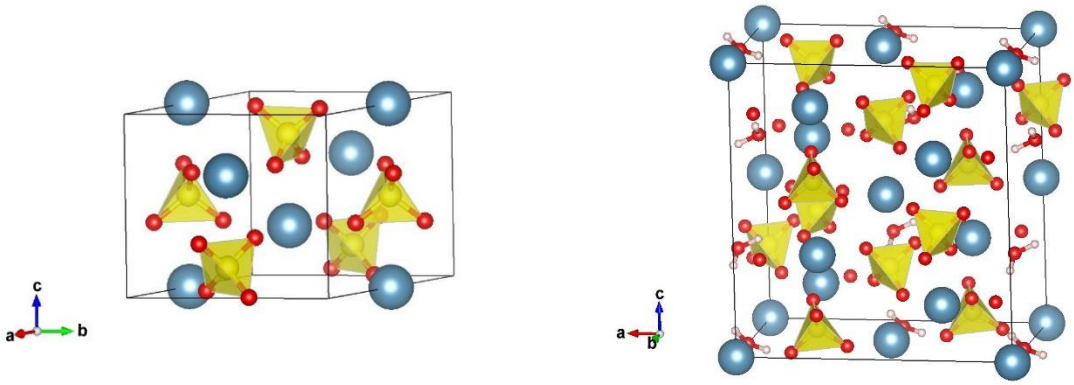

(**a**) (**b**)

Figure 2. Visualization of the a) $CaSO_4$-anhydrite that appears in *P6222* (no. 180); b) $CaSO_4$-hemihydrate in space group *C2* (no. 5), calculated with the GGA-PBE functional. Blue, yellow, red, and pink spheres denote calcium, sulphur, oxygen, and hydrogen atoms, respectively.

The only optimized structure within this group that crystallizes in a lower symmetry group is $CaSO_4$-hemihydrate [53]. This compound has been used as a building material for thousands of years and it can endure extreme conditions. It appears in space group *C2* (no. 5) with unit cell parameters of a=12.181, b=7.063, c=13.010 Å, and β=90.353, and the structure is visualized in Figure 2b. Sulphur atoms are surrounded by four oxygen atoms, and form three different tetrahedra with interatomic distances in a range of 1.5261 Å-O as the smallest distance, to 1.5422 Å-O as the largest interatomic distance, while there are also three different water molecules with distances between hydrogen and oxygen atoms of (H_1) 0.9852 Å-O, (H_2) 0.9898 Å-O, and (H_3) 0.9893 Å-O, respectively. The total energy of this modification calculated with two different functionals, GGA-PBE and the LDA-PZ are presented in Table 1, while full structural data on the GGA level of calculation are given in Table 2, respectively.

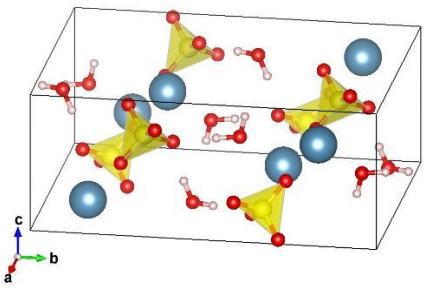

Figure 3. Visualization of the $CaSO_4x2H_2O$ in *C12/c1* (no. 15), calculated with the GGA-PBE functional. Blue, yellow, red, and pink spheres denote calcium, sulphur, oxygen, and hydrogen atoms, respectively.

The final optimized structure is the calcium sulphate dihydrate (gypsum), a material that contains water in the structure (unlike previously computed anhydrite). Anhydrite closely resembles gypsum, however, it is slightly harder and denser compared to gypsum. Gypsum crystallizes in space group *C12/c1* (no. 15) with unit cell parameters a=6.495, b=15.237, c=5.725Å and β=115.105, on the GGA-PBE level of calculation. Our DFT calculations concur with the literature data [54]. Within this structure, sulphur is in 4-fold coordination with oxygen and forms tetrahedra with interatomic distances of 2 × 1.5304 Å-O and 2 × 1.5409 Å-O, respectively. Oxygen atoms are connected to two hydrogen atoms making a water molecule, with distances of 0.9940 Å-O and 1.0013 Å-O, and the structure is presented in Figure 3.

Table 2. Full structural data of the most interesting modifications calculated with the GGA-PBE functional.

Modification	**Cell parameters (Å)**	**Position of atoms**
CaO *Fm-3m* (no. 225)	a= 4.828	Ca 0.00000 0.00000 0.00000 O 0.50000 0.50000 0.50000
CaOH *P-3m1* (no. 164)	a=3.613 c=4.974	Ca 0.00000 0.00000 0.00000 O 0.33333 0.66667 0.23120 H 0.33333 0.66667 0.42934
$CaSO_4$-anhydrite *P6222* (no. 180)	a=7.093 c=6.450	Ca 0.50000 0.00000 0.00000 S 0.50000 0.00000 0.50000 O 0.44708 0.13836 0.35497
$CaSO_4$-hemihydrate *C2* (no. 5)	a=12.181 b=7.063 c=13.010 β=90.353	Ca 0.000000 0.000000 0.000000 Ca 0.000000 0.041583 0.500000 Ca 0.229284 0.334845 0.832602 Ca 0.785512 0.355078 0.666962 S 0.774689 0.337691 0.918828 S 0.003088 0.015067 0.747868 S 0.225092 0.353110 0.582985 O 0.184487 0.879947 0.997289 O 0.177234 0.886982 0.487903 O 0.756804 0.677884 0.155160 O 0.747738 0.694063 0.660660 O 0.063107 0.140685 0.826257 O 0.566288 0.630726 0.327812 O 0.795609 0.511872 0.851283 O 0.803214 0.526497 0.350968 O 0.123944 0.289525 0.015938 O 0.129134 0.301407 0.511457 O 0.070755 0.883506 0.187990 O 0.081886 0.901355 0.681216 O 0.000000 0.656480 0.000000 O 0.957252 0.524710 0.693614 H 0.944784 0.572042 0.968707 H 0.953515 0.639334 0.737217 H 0.030584 0.525407 0.661366
$CaSO_4x2H_2O$ *C2/c* (no. 15)	a=6.495 b=15.237 c=5.725 β=115.105	Ca 0.00000 0.83275 0.75000 S 0.00000 0.32925 0.75000 O 0.70390 0.88624 0.92265 O 0.08718 0.27274 0.58994 O 0.79439 0.93198 0.41972 H 0.74821 0.91178 0.23796 H 0.75732 0.99546 0.41385

To investigate the $CaCO_3$ under extreme conditions, an *ab initio* data mining approach has been performed. High-pressure phases of calcite and aragonite, two different modifications of $CaCO_3$,

are optimized using the three different functionals (GGA-PBE, LDA-PZ, B3LYP). Calculated total and relative energies for the five high-pressure calcite and aragonite modifications are listed in Table 3.

Table 3. Calculated total and relative energies per formula unit for different $CaCO_3$ modifications.

Modifications	**GGA-PBE**		**LDA-PZ**		**B3LYP**	
	Total Energy (Eh)	**Relative Energy (kcal/mol)**	**Total Energy (Eh)**	**Relative Energy (kcal/mol)**	**Total Energy (Eh)**	**Relative Energy (kcal/mol)**
Calcite I ($CaCO_3$ I)	-941.1793	0	-937.9360	0	-941.4953	0
Calcite IIIa	-941.1740	3.326	-937.9357	0.188	-941.4888	4.079
Calcite IIIb	-941.1767	1.631	-937.9359	0.063	-941.4924	1.820
Calcite IIIc	-941.1775	1.129	-937.9339	1.318	-941.4934	1.192
Calcite VI	-941.1763	1.882	-937.9351	0.565	-941.4929	1.506
Aragonite	-941.1709	5.271	-937.9317	2.698	-941.4843	6.903

Calculated energies for all computed $CaCO_3$ modifications show similar rankings. Thus, the first modification, Calcite I ($CaCO_3$ I) has the lowest calculated energy regardless of the computational approach, while the highest computed energies were found in aragonite modification, which is expected as a high-pressure and/or high-temperature phase [55]. A structure with the highest calculated energy among calcite phases proved to be calcite IIIa modification using the GGA-PBE and the B3LYP functional, while calcite IIIc modification was energetically highest using the LDA-PZ functional (Table 3). On the other hand, Aragonite, another naturally occurring crystal form of $CaCO_3$, has the highest computed energies of all $CaCO_3$ modifications, which is expected at high pressures and/or temperatures.

The lowest energy minimum found using the data mining *ab initio* method was denoted as Calcite I ($CaCO_3$ I) modification. It crystallizes in space group *R3c* (SG no. 167) with unit cell parameters a=5.084 and c=17.002 Å, calculated using the GGA-PBE functional. It is visualized in Figure 4a, while full structural data are given in Table 4, on the GGA-PBE level of calculation. Within this structure calcium has 6-fold coordination by oxygen atoms, thus forming corner-connected octahedra. Besides, carbon atoms are in 3-fold coordination with oxygen atoms and form an equilateral triangle. Interatomic distances for calcium ions are 2.3862 Å-O and for carbon 1.3044 Å-O, respectively. The present calculation for the Calcite I type of structure agrees very well with previous reports [56-59] regardless of the computational approach. Furthermore, we have observed polytypic structures at high-pressure and/or high-temperature conditions which were recently discovered in $CaCO_3$ [60] and other chemical systems [61, 62].

Following modification on the energetic ranking using the GGA and the B3LYP functional is denoted as Calcite IIIc, which is visualized in Figure 3b. The Calcite IIIc modification is predicted within this study. We have started the DFT optimization from a metastable structure found at about 4 GPa, [63] and found a new Calcite IIIc type confirmed with all three *ab initio* methods. It crystallizes in space group *P321* (SG no. 150) with unit cell parameters a=5.062 c=8.631 Å, on the GGA-PBE level of calculation. Similar to the previous structure, calcium atoms are in 6-fold coordination with oxygen, however, form slightly distorted octahedra, with interatomic distances of (Ca_1) 2.4017 Å-O, (Ca_2) 2.3814 Å-O and 2.3863 Å-O, respectively. Octahedra positioned in the corners of the structure are connected to those inside the structure, but not to each other. Carbon atoms are 3-fold coordinated by oxygen and form an equilateral triangle, while distances between atoms are (C_1) 1.3043 Å-O and (C_2) 1.3046 Å-O. When calculated using the LDA-PZ functional, this structure proved to be much higher in energy.

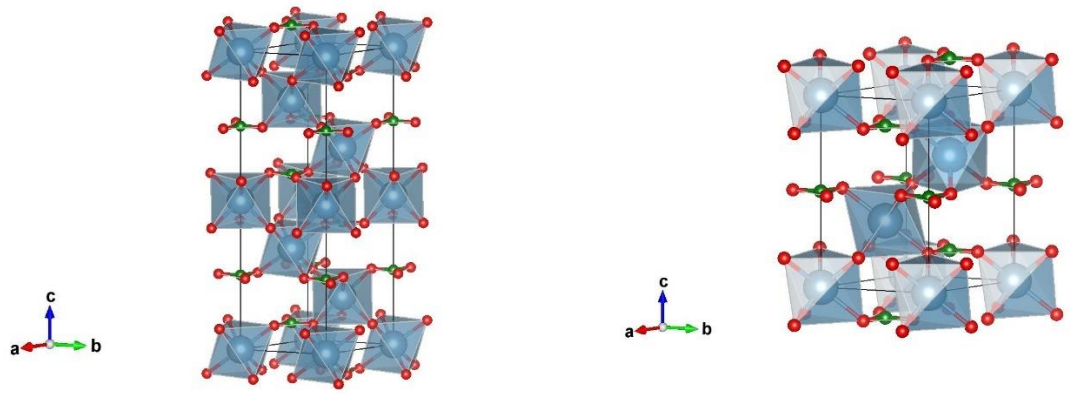

(**a**) (**b**)

Figure 4. Visualization of a) Calcite I ($CaCO_3$ I) modification in space group *R-3c* (no. 167); b) Calcite IIIc modification that appears in space group *P321* (SG no. 150). Blue, green, and red spheres denote calcium, carbon, and oxygen atoms, respectively.

Structure denoted as Calcite IIIb has a lower symmetry and appears in space group *P-1* (SG no. 2) with unit cell parameters a=6.418, b=6.635, c=6.474 Å, α=97.853, β=103.890, and γ=104.796, on the GGA-PBE level of calculation. This is an interesting modification, as calcium atoms are in 7-fold coordination with oxygen atoms, thus forming edge, and corner connected polyhedra (Figure 5a), with interatomic distances of (Ca_1) 2.3297 Å-O, 2.3595 Å-O, 2.3626 Å-O, 2.4340 Å-O, 2.4780 Å-O, 2.5773 Å-O, 2.6136 Å-O, and (Ca_2) 2.3178 Å-O, 2.3528 Å-O, 2.3804 Å-O, 2.3829 Å-O, 2.5002 Å-O, 2.5179 Å-O, 2.6824 Å-O, respectively. Carbon atoms are 3-fold coordinated by oxygen atoms and represent the center of the equilateral triangle, with interatomic distances of (C_1) 1.2993 Å-O, 1.3011 Å-O, 1.3012 Å-O and (C_2) 1.2915 Å-O, 1.3088 Å-O, 1.3168 Å-O.

Another low symmetry candidate that appears in space group *P-1* (SG no. 2) is referred to as Calcite VI modification, and it is visualized in Figure 5b with unit cell parameters a=3.870, b=5.156, c=6.661 Å, α=93.569, β=106.600, and γ=90.655, calculated using the GGA-PBE functional. Calcium atoms are 6-fold coordinated by oxygen and form distorted octahedra, while carbon remains in 3-fold coordination with oxygen. The interatomic distances are for Ca 2.3437 Å-O, 2.3772 Å-O, 2.3945 Å-O, 2.3987 Å-O, 2.4077 Å-O, 2.4576 Å-O, 2.7909 Å-O, and for C 1.2963 Å-O, 1.2997 Å-O, 1.3131 Å-O, respectively.

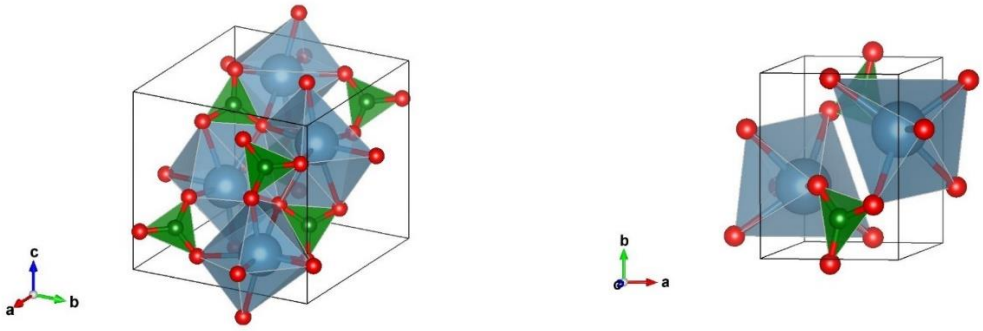

(**a**) (**b**)

Figure 5. Visualization of a) Calcite IIIb that appears in space group *P-1* (SG no. 2); b) Calcite VI in space group *P-1* (SG no. 2). Blue, green, and red spheres denote calcium, carbon, and oxygen atoms, respectively.

With the highest calculated energy using the GGA-PBE functional, there is another calcite modification denoted as Calcite IIIa that appears in space group *P-1* (SG no. 2) with unit cell

parameters a=6.422, b=7.775, c=12.764 Å, α=94.000, β=98.457, and γ=106.902. Within this structure, calcium is in 6-fold coordination and forms more or less distorted, corner-connected octahedra (Figure 6). Carbon atoms are positioned in the center of the planar group of oxygen atoms thus defining an equilateral triangle. The smallest interatomic distance for Ca_1 is 2.3974 Å-O, and it goes to the 2.4850 Å-O as the biggest distance, for Ca_2 these values are from 2.3271 Å-O to 2.5895 Å-O, for Ca_3 are from 2.3375 Å-O to 2.5313 Å-O, Ca_4 from 2.2785 Å-O to 2.5097 Å-O and for Ca_5 from 2.3921 Å-O to 2.4789 Å-O. As there are also five different carbon atoms, the distance between atoms for C_1 goes from 1.2818 Å-O to 1.3256 Å-O, C_2 from 1.2805 Å-O to 1.3143 Å-O, for C_3 from 1.2917 Å-O to 1.3123 Å-O, for C_4 from 1.2838 Å-O to 1.3203 Å-O and for the C_5 from 1.2862 Å-O to 1.3131 Å-O, respectively.

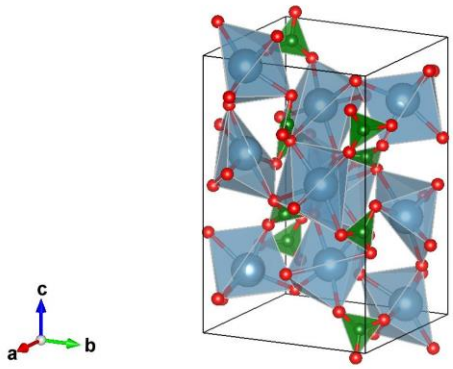

Figure 6. Visualization of the calcite IIIa modification that appears in space group *P-1* (SG no.2). Blue, green, and red spheres denote calcium, carbon, and oxygen atoms, respectively.

Table 4. Structure parameters of $CaCO_3$ phases calculated using the GGA-PBE functional.

Modifications and space group	**Cell parameters**	**Position of atoms**
Calcite I ($CaCO_3$ I) *R-3c* (SG no.167)	a=5.084 c=17.002	Ca 0.00000 0.00000 0.00000 C 0.00000 0.00000 0.25000 O -0.33333 0.07678 0.58333
Calcite IIIa *P-1* (SG no.2)	a=6.422 b=7.775 c=12.764 α=94.000 β=98.457 γ=106.902	Ca 0.83462 0.64293 0.55924 Ca 0.27128 0.87970 0.38168 Ca 0.51488 0.47742 0.78791 Ca 0.41574 0.93374 0.82704 Ca 0.01694 0.74906 0.02117 C 0.99275 0.51712 0.79004 C 0.37539 0.68572 0.59994 C 0.55816 0.73875 0.00473 C 0.04951 0.03662 0.20200 C 0.71839 0.84037 0.38697 O 0.40827 0.81383 0.02410 O 0.92103 0.50234 0.88222 O 0.19745 0.59060 0.78622 O 0.64116 0.87984 0.47193 O 0.84181 0.45775 0.70391 O 0.20124 0.66297 0.52665 O 0.46198 0.55223 0.60636 O 0.62683 0.75132 0.91286 O 0.16557 0.92323 0.19489 O 0.05542 0.12624 0.29132 O 0.91926 0.04956 0.11465 O 0.90052 0.80032 0.39877 O 0.65061 0.66033 0.07542

		O 0.46275 0.83329 0.66278 O 0.59692 0.82731 0.29282
Calcite IIIb *P-1* (SG no. 2)	a=6.418 b=6.635 c=6.474 α=97.853 β=103.890 γ=104.796	Ca 0.51812 0.77288 0.67988 Ca 0.01562 0.27830 0.78316 C 0.98359 0.23170 0.27066 C 0.53432 0.73685 0.22034 O 0.99382 0.62867 0.85160 O 0.59827 0.16370 0.71566 O 0.60747 0.60947 0.33919 O 0.09011 0.08982 0.26329 O 0.85879 0.23751 0.40146 O 0.39323 0.23050 0.94549
Calcite IIIc *P321* (SG no. 150)	a=5.062 c=8.631	Ca 0.00000 0.00000 0.00000 Ca 0.66667 0.33333 0.33496 C 0.00000 0.00000 0.50000 C 0.33333 0.66667 0.17030 O 0.25761 0.25761 0.50000 O 0.33133 0.92334 0.16998
Calcite VI *P-1* (SG no. 2)	a=3.870 b=5.156 c=6.661 α=93.569 β=106.600 γ=90.655	Ca 0.92367 0.67890 0.74171 C 0.50368 0.80485 0.24598 O 0.70086 0.63736 0.36650 O 0.58346 0.05181 0.27417 O 0.21578 0.71498 0.10313
Aragonite *Pnma* (SG no. 62)	a=5.769 b=5.061 c=8.103	Ca 0.73787 0.75000 0.58612 C 0.42084 0.25000 0.76246 O 0.41324 0.25000 0.92198 O 0.41753 0.02722 0.68106

Aragonite is another naturally occurring crystal form of calcium carbonate that is stable at high pressures and/or temperatures [55, 64]. The aragonite type modification crystallizes in space group *Pnma* (SG no. 62) with calculated unit cell parameters a=5.769, b=5.061, and c=8.103 Å, on the GGA-PBE level of calculation. Calcium atoms are in 7-fold coordination with oxygen atoms, thus forming edge-connected polyhedra, and interatomic distances are 1 × 2.4127 Å-O, 2 × 2.4447 Å-O, 2 × 2.5694 Å-O, 2 × 2.6004 Å-O, respectively. Carbon atoms are in 3-fold coordination by oxygen atoms and form equilateral triangles with interatomic distances of 1 × 1.2933 Å-O and 2 × 1.3064 Å-O, respectively. The structure is visualized in Figure 7, while full structural data are given in Table 4, calculated with the GGA-PBE functional.

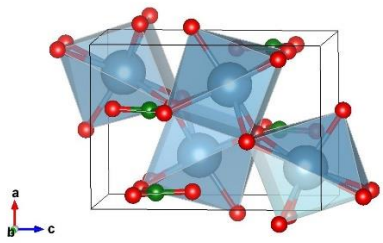

Figure 7. Visualization of the Aragonite that appears in space group *Pnma* (SG no. 62). Blue, green, and red spheres denote calcium, carbon, and oxygen atoms, respectively.

4. Conclusion

To investigate the behavior of calcite and gypsum modifications at standard and extreme conditions of pressure and temperature, a data-mining *ab initio* approach has been performed. Local structure optimizations have been carried out using the DFT approach with LDA-PZ and GGA-PBE functionals, as well as combined with the hybrid B3LYP functional. In total five gypsum-related

compounds and modifications, and six $CaCO_3$ modifications have been investigated. Computed structural and energetic properties of different gypsum phases are presented and in agreement with previous reports. In the case of the $CaCO_3$ chemical system, the calcite I ($CaCO_3$ I) phase has the lowest calculated total energy regardless of the computational approach, while aragonite modification appears energetically the highest, which is expected as a high-pressure phase. It is of great importance to the findings of polytypic behaviors in $CaCO_3$ at high pressures, which has been recently confirmed. Moreover, this study shows new predicted calcite IIIc phase in the high symmetry *P321* (no. 150) space group, which should withstand extremely high-pressure conditions. The discovery of these new modifications with possible use in extreme conditions and their eventual synthesis might have possible very wide industrial and technological applications.

Acknowledgments

This work was financially supported by the Ministry of Science, Technological Development and Innovation of the Republic of Serbia through Contract No. 451-03-47/2023-01/200017. The authors are grateful to Prof. R. Dovesi, Prof. K. Doll, and Crystal Solutions for software support with CRYSTAL code. The authors thank the Max Planck Institute for Solid State Research, Stuttgart, Germany, for collaboration and for providing computational support.

References

[1] Y. Ma, Q. Zhou, Z. He, F. Li, K. Yang, Q. Cui, G. Zou, High-pressure and high-temperature study of the phase transition in anhydrite, Journal of Physics: Condensed Matter, 19 (2007) 425221.
[2] L. Yang, L. Dai, H. Li, H. Hu, Y. Zhuang, K. Liu, C. Pu, M. Hong, Pressure-induced structural phase transition and dehydration for gypsum investigated by Raman spectroscopy and electrical conductivity, Chemical Physics Letters, 706 (2018) 151-157.
[3] S.J. Brotton, R.I. Kaiser, In situ Raman spectroscopic study of gypsum ($CaSO_4 \cdot 2H_2O$) and epsomite ($MgSO_4 \cdot 7H_2O$) dehydration utilizing an ultrasonic levitator, The Journal of Physical Chemistry Letters, 4 (2013) 669-673.
[4] C.-J. Liu, H.-F. Zheng, In situ observation of gypsum-anhydrite transition at high pressure and high temperature, Chinese Physics Letters, 29 (2012) 049101.
[5] S. Bradbury, Q. Williams, X-ray diffraction and infrared spectroscopy of monazite-structured $CaSO_4$ at high pressures: Implications for shocked anhydrite, Journal of Physics and Chemistry of Solids, 70 (2009) 134-141.
[6] P. Comodi, A. Kurnosov, S. Nazzareni, L. Dubrovinsky, The dehydration process of gypsum under high pressure, Physics and Chemistry of Minerals, 39 (2012) 65-71.
[7] J. Kirtley, V. Leichner, B.R. Anderson, H. Eilers, A comparison of pulsed and continuous lasers for high-temperature Raman measurements of anhydrite, Journal of Raman Spectroscopy, 49 (2018) 862-871.
[8] T. Fujii, H. Ohfuji, T. Inoue, Phase relation of CaSO4 at high pressure and temperature up to 90 GPa and 2300 K, Physics and Chemistry of Minerals, 43 (2016) 353-361.
[9] E. Knittle, W. Phillips, Q. Williams, An infrared and Raman spectroscopic study of gypsum at high pressures, Physics and Chemistry of Minerals, 28 (2001) 630-640.
[10] M. Merlini, M. Hanfland, W. Crichton, $CaCO_3$-III and $CaCO_3$-VI, high-pressure polymorphs of calcite: possible host structures for carbon in the Earth's mantle, Earth and Planetary Science Letters, 333 (2012) 265-271.
[11] K. Suito, J. Namba, T. Horikawa, Y. Taniguchi, N. Sakurai, M. Kobayashi, A. Onodera, O. Shimomura, T. Kikegawa, Phase relations of $CaCO_3$ at high pressure and high temperature, American Mineralogist, 86 (2001) 997-1002.
[12] D. Druzhbin, S.V. Rashchenko, A. Shatskiy, W.A. Crichton, New High-Pressure and High-Temperature $CaCO_3$ Polymorph, ACS Earth and Space Chemistry, (2022).
[13] D. Huang, H. Liu, M.-Q. Hou, M.-Y. Xie, Y.-F. Lu, L. Liu, L. Yi, Y.-J. Cui, Y. Li, L.-W. Deng, Elastic properties of $CaCO_3$ high pressure phases from first principles, Chinese Physics B, 26 (2017) 089101.

[14] X. Li, Z. Zhang, J.F. Lin, H. Ni, V.B. Prakapenka, Z. Mao, New high-pressure phase of $CaCO_3$ at the topmost lower mantle: Implication for the deep-mantle carbon transportation, Geophysical Research Letters, 45 (2018) 1355-1360.
[15] S.S. Santos, M.L. Marcondes, J.F. Justo, L.V. Assali, Calcium carbonate at high pressures and high temperatures: a first-principles investigation, Physics of the Earth and Planetary Interiors, 299 (2020) 106327.
[16] L. Bayarjargal, C.-J. Fruhner, N. Schrodt, B. Winkler, $CaCO_3$ phase diagram studied with Raman spectroscopy at pressures up to 50 GPa and high temperatures and DFT modeling, Physics of the Earth and Planetary Interiors, 281 (2018) 31-45.
[17] P.N. Gavryushkin, N. Sagatov, A.B. Belonoshko, M.V. Banaev, K.D. Litasov, Disordered aragonite: The new high-pressure, high-temperature phase of $CaCO_3$, The Journal of Physical Chemistry C, 124 (2020) 26467-26473.
[18] M. Hou, Q. Zhang, R. Tao, H. Liu, Y. Kono, H.-k. Mao, W. Yang, B. Chen, Y. Fei, Temperature-induced amorphization in $CaCO_3$ at high pressure and implications for recycled $CaCO_3$ in subduction zones, Nature communications, 10 (2019) 1-8.
[19] A.R. Oganov, C.W. Glass, S. Ono, High-pressure phases of $CaCO_3$: crystal structure prediction and experiment, Earth and Planetary Science Letters, 241 (2006) 95-103.
[20] S. Ono, T. Kikegawa, Y. Ohishi, High-pressure transition of $CaCO_3$, American Mineralogist, 92 (2007) 1246-1249.
[21] G. Bergerhoff, I. Brown, F. Allen, Crystallographic databases, International Union of Crystallography, Chester, 360 (1987) 77-95.
[22] D. Zagorac, H. Müller, S. Ruehl, J. Zagorac, S. Rehme, Recent developments in the Inorganic Crystal Structure Database: theoretical crystal structure data and related features, Journal of applied crystallography, 52 (2019) 918-925.
[23] J. Zagorac, D. Zagorac, M. Rosić, J.C. Schön, B. Matović, Structure prediction of aluminum nitride combining data mining and quantum mechanics, CrystEngComm, 19 (2017) 5259-5268.
[24] D. Zagorac, J.C. Schön, M. Jansen, Identification of promising chemical systems for the synthesis of new materials structure types: An ab initio minimization data mining approach, Processing and Application of Ceramics, 7 (2013) 37-41.
[25] T. Škundrić, D. Zagorac, J.C. Schön, M. Pejić, B. Matović, Crystal structure prediction of the novel Cr_2SiN_4 compound via global optimization, data mining, and the PCAE method, Crystals, 11 (2021) 891.
[26] D. Zagorac, J.B. Zagorac, K. Doll, M. Čebela, B. Matović, Extreme pressure conditions of bas based materials: Detailed study of structural changes, band gap engineering, elastic constants and mechanical properties, Processing and Application of Ceramics, 13 (2019) 401-410.
[27] D. Jovanović, J.B. Zagorac, B. Matović, A.R. Zarubica, D. Zagorac, Structural, electronic and mechanical properties of superhard B4C from first principles, Journal of Innovative Materials in Extreme Conditions, 1 (2020) 19-27.
[28] J.B. Zagorac, D. Zagorac, D. Jovanović, M. Pejić, T. Škundrić, B. Matović, Ab Initio Investigations and Behaviour of the α-Ce_2ON_2 Phase in the Extreme Pressure Conditions, Journal of Innovative Materials in Extreme Conditions, 2 (2021) 36-43.
[29] J.C. Schön, Energy Landscape Concepts for Chemical Systems under Extreme Conditions, Journal of Innovative Materials in Extreme Conditions, 2 (2021) 5-57.
[30] D. Zagorac, K. Doll, J. Schön, M. Jansen, Ab initio structure prediction for lead sulfide at standard and elevated pressures, Physical Review B, 84 (2011) 045206.
[31] A.A. Sokol, C.R.A. Catlow, M. Miskufova, S.A. Shevlin, A.A. Al-Sunaidi, A. Walsh, S.M. Woodley, On the problem of cluster structure diversity and the value of data mining, Physical Chemistry Chemical Physics, 12 (2010) 8438-8445.
[32] G. Ceder, D. Morgan, C. Fischer, K. Tibbetts, S. Curtarolo, Data-mining-driven quantum mechanics for the prediction of structure, MRS bulletin, 31 (2006) 981-985.
[33] R. Dovesi, A. Erba, R. Orlando, C.M. Zicovich-Wilson, B. Civalleri, L. Maschio, M. Rérat, S. Casassa, J. Baima, S. Salustro, Quantum-mechanical condensed matter simulations with CRYSTAL, Wiley Interdisciplinary Reviews: Computational Molecular Science, 8 (2018) e1360.

[34] R. Dovesi, R. Orlando, B. Civalleri, C. Roetti, V.R. Saunders, C.M. Zicovich-Wilson, CRYSTAL: a computational tool for the ab initio study of the electronic properties of crystals, Zeitschrift für Kristallographie-Crystalline Materials, 220 (2005) 571-573.
[35] R. Dovesi, F. Pascale, B. Civalleri, K. Doll, N.M. Harrison, I. Bush, P. D'arco, Y. Noël, M. Rérat, P. Carbonnière, The CRYSTAL code, 1976–2020 and beyond, a long story, The Journal of chemical physics, 152 (2020) 204111.
[36] J.P. Perdew, K. Burke, M. Ernzerhof, Generalized gradient approximation made simple, Physical review letters, 77 (1996) 3865.
[37] J.P. Perdew, A. Zunger, Self-interaction correction to density-functional approximations for many-electron systems, Physical Review B, 23 (1981) 5048.
[38] A.D. Becke, Density-functional thermochemistry. III. The role of exact exchange, The Journal of Chemical Physics, 98 (1993) 5648-5652.
[39] M. Catti, A. Pavese, V. Saunders, Elastic constants and electronic structure of fluorite (CaF_2): an ab initio Hartree-Fock study, Journal of Physics: Condensed Matter, 3 (1991) 4151.
[40] M. Catti, A. Pavese, R. Dovesi, V. Saunders, Static lattice and electron properties of $MgCO_3$ (magnesite) calculated by ab initio periodic Hartree-Fock methods, Physical Review B, 47 (1993) 9189.
[41] M.D. Towler, N.L. Allan, N.M. Harrison, V.R. Saunders, W.C. Mackrodt, E. Aprà, Ab initio study of MnO and NiO, Physical Review B, 50 (1994) 5041-5054.
[42] D. Zagorac, J. Schön, J. Zagorac, M. Jansen, Prediction of structure candidates for zinc oxide as a function of pressure and investigation of their electronic properties, Physical Review B, 89 (2014) 075201.
[43] R. Dovesi, C. Ermondi, E. Ferrero, C. Pisani, C. Roetti, Hartree-Fock study of lithium hydride with the use of a polarizable basis set, Physical Review B, 29 (1984) 3591.
[44] D. Jovanović, D. Zagorac, J.C. Schön, B. Milovanović, J. Zagorac, A new theoretical model for hexagonal ice, Ih (d), from first principles investigations, Zeitschrift für Naturforschung B, 75 (2020) 125-128.
[45] W. Perger, J. Criswell, B. Civalleri, R. Dovesi, Ab-initio calculation of elastic constants of crystalline systems with the CRYSTAL code, Computer Physics Communications, 180 (2009) 1753-1759.
[46] R. Hundt, J.C. SchoÈn, A. Hannemann, M. Jansen, Determination of symmetries and idealized cell parameters for simulated structures, Journal of applied crystallography, 32 (1999) 413-416.
[47] A. Hannemann, R. Hundt, J. Schön, M. Jansen, A new algorithm for space-group determination, Journal of applied crystallography, 31 (1998) 922-928.
[48] R. Hundt, A. Kplot, Program for Plotting and Analyzing Crystal Structures, Technicum Scientific Publishing, Stuttgart, 2016.
[49] K. Momma, F. Izumi, VESTA 3 for three-dimensional visualization of crystal, volumetric and morphology data, Journal of applied crystallography, 44 (2011) 1272-1276.
[50] W. Gerlach, Die gitterstruktur der erdalkalioxyde, Zeitschrift für Physik, 9 (1922) 184-192.
[51] W.R. Busing, H.A. Levy, Neutron diffraction study of calcium hydroxide, The Journal of chemical physics, 26 (1957) 563-568.
[52] O. Flörke, Crystallographic and X-Radiographic Investigations in the System CaSO4–CaSO4. 2H2O, Neves Jahrbuch fur Mineralogie, Geologie und Paleontologie, Abhandlung, 84 (1952) 189-240.
[53] W. Abdel, Bestimmung der Kristallstruktur von $CaSO_4(H_2O)_{0,5}$ mit Röntgenbeugungsmethoden und mit Potentialprofil-Rechnungen, Zeitschrift für Kristallographie-Crystalline Materials, 205 (1993) 99-116.
[54] R. Khasanov, N. Nizamutdinov, N. Khasanova, A. Gubaĭdullin, V. Vinokurov, Low-temperature dehydration of gypsum single crystals, Crystallography Reports, 53 (2008) 806-811.
[55] D. Bevan, E. Rossmanith, D.K. Mylrea, S.E. Ness, M.R. Taylor, C. Cuff, On the structure of aragonite–Lawrence Bragg revisited, Acta Crystallographica Section B: Structural Science, 58 (2002) 448-456.
[56] S.M. Antao, I. Hassan, W.H. Mulder, P.L. Lee, B.H. Toby, In situ study of the orientational disorder in calcite, Physics and Chemistry of Minerals, 36 (2009) 159-169.

[57] V. Borodin, V. Lyutin, V. Ilyukhin, N. Belov, The isomorphous series calcite-otavite, Doklady Akademii Nauk SSSR, 245 (1979) 1099-1101.
[58] H. Chessin, W.C. Hamilton, B. Post, Position and thermal parameters of oxygen atoms in calcite, Acta Crystallographica, 18 (1965) 689-693.
[59] S.M. Antao, I. Hassan, Temperature dependence of the structural parameters in the transformation of aragonite to calcite, as determined from in situ synchrotron powder X-ray-diffraction data, The Canadian Mineralogist, 48 (2010) 1225-1236.
[60] P.N. Gavryushkin, A.B. Belonoshko, N. Sagatov, D. Sagatova, E. Zhitova, M.G. Krzhizhanovskaya, A. Recnik, E.V. Alexandrov, I.V. Medrish, Z.I. Popov, Metastable structures of CaCO3 and their role in transformation of calcite to aragonite and postaragonite, Crystal Growth & Design, 21 (2020) 65-74.
[61] D. Zagorac, J. Schön, J. Zagorac, M. Jansen, Theoretical investigations of novel zinc oxide polytypes and in-depth study of their electronic properties, RSC Advances, 5 (2015) 25929-25935.
[62] D. Zagorac, J. Zagorac, J.C. Schoen, N. Stojanović, B. Matović, ZnO/ZnS (hetero) structures: Ab initio investigations of polytypic behavior of mixed ZnO and ZnS compounds, Acta Crystallographica Section B: Structural Science, Crystal Engineering and Materials, 74 (2018) 628-642.
[63] J.R. Smyth, T.J. Ahrens, The crystal structure of calcite III, Geophysical Research Letters, 24 (1997) 1595-1598.
[64] T. Pilati, F. Demartin, C. Gramaccioli, Lattice-dynamical estimation of atomic displacement parameters in carbonates: calcite and aragonite $CaCO_3$, dolomite $CaMg(CO_3)_2$ and magnesite $MgCO_3$, Acta Crystallographica Section B: Structural Science, 54 (1998) 515-523.